NEGATIVE ION FORMATION AND ENERGY LOSSES IN MOLECULAR GASES

FINAL TECHNICAL REPORT

for the

ADVANCED RESEARCH PROJECTS AGENCY

ARPA Order No. 1479
Contract No. N00014-67-A-0097-0008
Program Code NR012-133

Principal Investigator:
George J. Schulz
Professor, Applied Science
Department of Engineering and Applied Science
YALE UNIVERSITY
New Haven, Connecticut 06520
Telephone: 203/436-3046

Security Classification

DOCUMENT CONTROL DATA - R & D

Security classification of title, body of abstract and indexing annotation must be entered when the overall report is classified)

1 ORIGINATING ACTIVITY (Corporate author)

YALE UNIVERSITY
Department of Engineering and Applied Science

2a. REPORT SECURITY CLASSIFICATION

Unclassified

2b. GROUP

3 REPORT TITLE

4 DESCRIPTIVE NOTES (Type of report and inclusive dates)

Final Report, August 1972

5 AUTHOR(S) (First name, middle initial, last name)

George J. Schulz

6 REPORT DATE

August 15, 1972

7a. TOTAL NO. OF PAGES

28

7b. NO. OF REFS

8a. CONTRACT OR GRANT NO.

N00014-67-A-0097-0008

b. PROJECT NO.

c.

d.

9a. ORIGINATOR'S REPORT NUMBER(S)

9b. OTHER REPORT NO(S) (Any other numbers that may be assigned this report)

10. DISTRIBUTION STATEMENT

Distribution of this document is unlimited.

11 SUPPLEMENTARY NOTES

12. SPONSORING MILITARY ACTIVITY

ARPA

13 ABSTRACT

This report describes, in summary form, various cross section measurements for electron impact at low energies: Vibrational cross sections in N_2, NO, CO_2; dissociative attachment in the temperature range 300-1000° for O_2 and CO_2; the temperature dependence of three-body attachment in O_2; the temperature dependence of total electron attachment near zero energy in SF_6, CCl_4, $CFCl_3$, CH_2Br_2, CH_3I, $CHCl_3$, CF_3Br, CH_3Br.

DD FORM 1 NOV 65 1473 (PAGE 1)

0102 014 6600

Security Classification

Security Classification

14 KEY WORDS	LINK A		LINK B		LINK C	
	ROLE	WT	ROLE	WT	ROLE	WT
cross sections						
molecules						
vibrational						
attachment						
electrons						
temperature						
N_2						
CO_2						
NO						
O_2						
SF_6						
CCl_4						
$CFCl_3$						
CH_2Br_2						
CH_3I						
$CHCl_3$						
CF_3Br						
CH_3Br						

NEGATIVE ION FORMATION AND ENERGY LOSSES IN MOLECULAR GASES

Table of Contents:

I. INTRODUCTION

In this final report we review briefly the accomplishments of our group in the area of ARPA sponsored work. The discussion of each topic is short, and the reader is referred to published material if he desires more detail. A list of references to our work is appended.

Most of the processes discussed in this report are important in two distinct areas of ARPA interest, namely in reentry in the presence and in the absence of seeding, and in an understanding of high-powered CO_2 lasers and similar molecular laser systems.

The Role of Gas Temperature

In order to measure processes under circumstances which are directly applicable to wakes at reentry (where the gas temperature is high), we decided some time ago that it is imperative to measure cross sections and rate coefficients at elevated temperatures. The elevated temperature alters the populations of vibrational and rotational levels

of the target molecule, and we find that very often the electron impact cross sections depend markedly on the population of these vibrational and rotational levels, i.e., on the gas temperature. Our own experiments encompass the range of temperatures from about 100°K to 2000°K.

It should be noted that the considerations outlined above are much more general than would appear. The temperature dependence of reaction rates must also be considered when one analyzes gas discharges, and especially when one wishes to analyze the reactions taking place in high-power molecular lasers. Such devices often contain high densities of vibrationally excited molecules and the reactions of these with the electrons must be considered. This is the reason why we became interested in studying CO_2, which is the active medium in the highest efficiency laser invented to date.

II. EXPERIMENTAL TUBE FOR NEGATIVE ION STUDIES AND VIBRATIONAL EXCITATION

Figure 1 is a schematic diagram of the experimental tube employed in some of the studies. A directly heated, thoria-coated iridium filament emits electrons whose energy distribution is reduced by use of the retarding-potential-difference method. A permanent magnet provides a magnetic field along the axis of the electron beam. The magnetic field can be varied between 400-1200 G by moving the pole faces. The collision chamber is a cylindrical iridium oven, 10 mm in diameter, 0.05 mm in thickness, which can be heated by the passage of a direct current. A current of 60 A is needed to attain a temperature of 950°K. A cylindrical iridium heat shield surrounds the collision chamber, to minimize heat losses by radiation. Mounted inside the collision chamber is a pair of iridium parallel-plate collectors for the total collection of ions. All electrodes, with the exception of the iridium parts and the electron collector, are gold plated to minimize contact potential differences and to maintain field uniformity. The electron collector is plated with an electrolytically deposited layer of platinum black to minimize reflection of electrons. The ion collectors and the electron collector are provided with guard plates to minimize current leakage across insulators. The electrical insulation for the electron gun is provided by sapphire balls, and for the ion collector by fused alumina and quartz. The whole tube is mounted on a fused alumina plate. The system is baked at 400°C for 24 hours, and a background pressure of 10^{-9} torr is obtained.

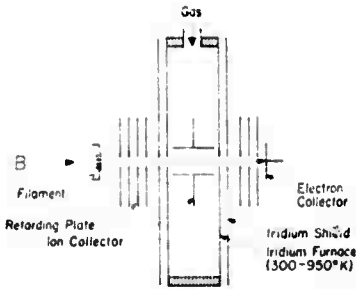

FIG. 1.

Gas is introduced into the collision chamber through a 2.5 mm tube, and the gas effusing through the holes in the collision chamber is differentially

pumped using a 4-inch diffusion pump. The tube is isolated from the pumping system by a liquid-nitrogen trap.

A sine wave of frequency 14 Hz and a peak-to-peak amplitude 80 mV is applied to the retarding electrode of the gun. Ions which are produced in the collision region are extracted by the parallel-plate collectors and passed through a high-value resistor, typically $10^{10}\Omega$. The resulting signal is applied to the input of a Keithley-301 operational amplifier which is used as an impedance match with unity voltage gain. In this mode, the amplifier has an input impedance of $10^{14}\Omega$ shunted by 0.1 $\mu\mu$F. The output of the operations amplifier is applied to a synchronous detector which selects signals of the correct frequency (14 Hz) and phase, so that the ion signal detected is that produced by electrons with an energy spread of about 80 mV. A similar lock-in amplifier is used to monitor the transmitted electron current. The collision-chamber potential is driven by the voltage from a ramp generator, which also drives the X axis of a two-pen X-Y recorder, while the signals from the synchronous detectors are displayed on the Y axis. This provides a plot of retarding-potential-difference ion current and transmitted RPD electron current as a function of incident electron energy.

The temperature of the furnace is determined primarily from the change of the positive-ion current in helium, as a function of furnace current. A constant mass flow of helium is maintained, and thus the density of helium (and hence the positive-ion current) is proportional to $T^{-\frac{1}{2}}$, where T is the absolute temperature. Molecular flow through the orifices is maintained by keeping the density in the furnace low. A spot check with an iridium/iridium-rhodium thermocouple attached to the furnace confirms the temperature scale within 2% up to a temperature of 550°K, and gives a temperature 6% higher at 800°K.

III. MODES OF OPERATION

The tube described previously can be operated in two distinct modes, giving information about two distinct processes. In one mode of operation, negative ion cross sections can be determined, and in the other mode the trapped-electron method is used for determining vibrational cross sections. Thus, a single tube gives us a great deal of information regarding low-energy electron loss processes in gases. A simple change of applied potentials alters the mode of operation.

IV. DISSOCIATIVE ATTACHMENT IN O_2 AT "ROOM TEMPERATURE"

The production of O^-/O_2 at "room temperature," i.e., with the oven inoperative, is found to have an onset of 4.4 $\pm$ 0.1 eV and a peak at 6.7 eV, in excellent agreement with previous data. The electron-energy scale and the electron-energy distribution are determined from retarding curves at the input and output of the collision chamber, respectively. The energy scale determined from retarding curves is in good agreement ($\pm$ 0.1 eV) with the energy scale determined from the onset of Xe^+ ions in pure xenon and mixtures of xenon and carbon dioxide, at both room temperature and at elevated temperatures. The electron energy distribution has a full width at half-maximum of about 0.08 eV.

The relative cross section for dissociative attachment at all temperatures is determined from the ratio of negative to positive ions.

The cross section for O^- formation from O_2 is well established to be 1.3×10^{-18} cm^2, and in fact it appears that this value, not being afflicted by errors resulting from secondary electron ejection, may be more reliable than some positive-ion cross sections. When we use the data of Tate and Smith [Phys. Rev. 39, 270 (1932)] or our own value for normalizing the ratio of negative to positive ions found in the present experiment, we obtain values of 1.28×10^{-18} and 1.30×10^{-18} cm^2 for the dissociative-attachment cross section in O_2.

V. TEMPERATURE DEPENDENCE OF DISSOCIATIVE ATTACHMENT CROSS SECTIONS IN O_2

The variation of the peak of the dissociative-attachment cross section as a function of temperature is shown in Fig. 2. It is observed that there is a very small increase in the cross section, up to the highest temperature used in the present experiment. The temperature range of the present experiment is limited by leakage across the insulators of the ion collector and by electron emission from the furnace.

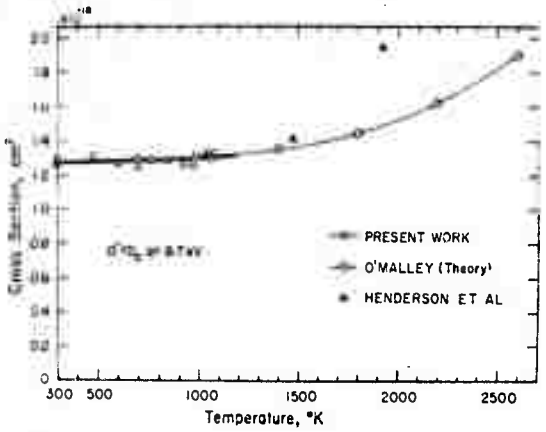

FIG. 2.

The triangles of Fig. 2 are obtained from the recent paper by Henderson, Fite and Brackmann [Phys. Rev. 183, 157 (1969)]. Normalized to our value of 1.28×10^{-18} cm^2 at room temperature, the open circles of Fig. 2 show the theoretical points obtained by O'Malley [Phys. Rev. 155, 59 (1967)] from a parametrization study of the O^-/O_2 process. His data are normalized to our value at room temperature.

Figure 3 presents the shift in onset of production of O^- for O_2, together with the shift in the location of the peak of the cross section, as a function of gas temperature. The onset moves to lower energy linearly with increasing temperature, but there is little shift in the energy at which the peak of the cross section occurs. The open circles in Fig. 3 have been calculated by O'Malley, and the triangles are the ex-

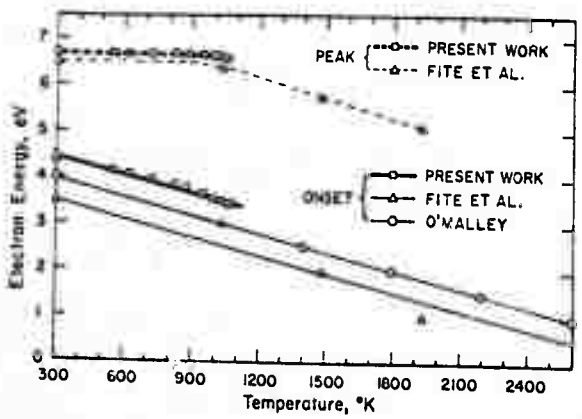

FIG. 3.

perimental data of Fite, Brackmann and Henderson, which are in essential agreement with their more recent measurements. The absolute energy difference between the present data and those of Fite et al. occurs because the energy spread of the electrons in their apparatus is larger than in the present experiment. The slope of O'Malley's theoretical shift in onset is in excellent agreement with our results, and in fact O'Malley's curve could have been raised upward to coincide completely with our results.

VI. DISSOCIATIVE ATTACHMENT CROSS SECTIONS IN CO_2

Figure 4 shows the energy dependence of the cross section for production of O^- from CO_2 at three different gas temperatures. It is seen that the onsets for production of O^-/CO_2 are shifted to lower energies as the temperature of the gas is raised, that both peaks broaden, and that there is a change in the peak cross section. The change in the peak cross section is illustrated more clearly in Fig. 5. The most striking feature of Fig. 5 is the initial fall in the cross section of the 8.2 eV peak, which then levels out and finally increases. The temperature dependence of the peak at 4.4 eV shows the expected behavior.

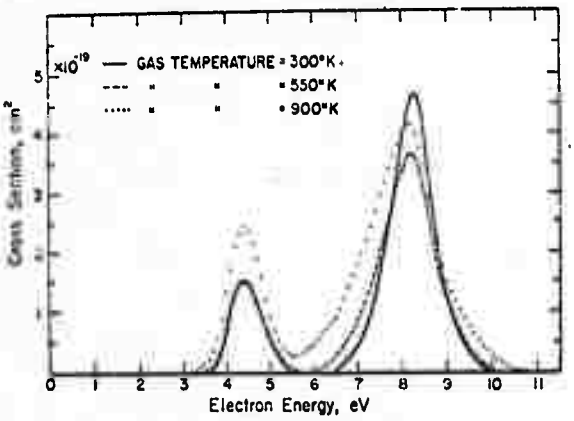

FIG. 4.

If one integrates the area under the 8.2 eV peak, it is found that the area remains constant until a temperature of 550°K is reached. The energy-integrated cross section (note that the right-hand scale is applicable to the integrated cross section) is also shown in Fig. 5. It is obvious from Fig. 4 that the area under the 4.4 eV peak also remains essentially constant to 550°K. It is found that the widths of both peaks at half-maximum increase monotonically as a function of temperature, but the

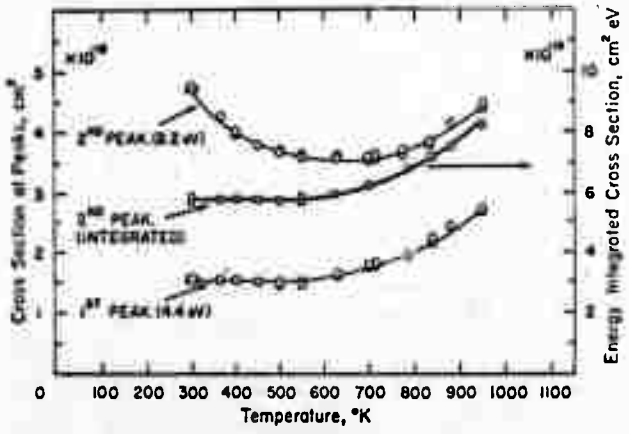

FIG. 5.

width of the second peak increases much faster than the first peak.

The onsets for production of O^- from CO_2, as a function of temperature, are shown in Fig. 6. In order to ensure that the electron energy scale does not shift as the temperature is changed, these experiments are performed in mixtures of Xe and CO_2. We establish the electron energy scale from electron retarding curves, and we use the onset of Xe^+ to confirm the energy scale. It is difficult to locate the energy of the onset of the second peak above 550°K because above this temperature the second onset overlaps the tail of the first peak, but no such problem exists with the location of the first onset. Figure 6 shows clearly that the onset for negative-ion production is strongly dependent on gas temperature. Negative ions are formed with zero kinetic energy at the first onset. Thus, the onset energy should give the difference between the dissociation energy D, and the electron affinity of oxygen A. The accepted value for D-A is 4.1 eV, and Fig. 6 shows that when the onset of the 4.4 eV peak is extrapolated to 0°K, an extrapolated onset of 4.1 $\pm$ 0.05 eV is actually observed. Thus, only the extrapolated onset of negative-ion formation is in agreement with accepted molecular parameters, and it is clear that one must study the temperature dependence of onsets before one can determine electron affinities from onsets of ions. It is expected that many of the discrepancies in the literature are caused by this type of temperature effect.

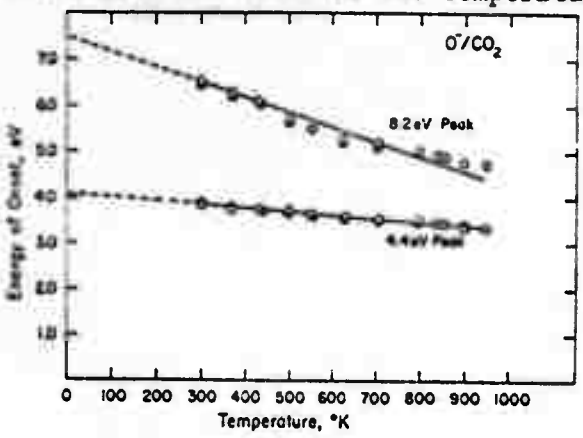

Fig. 6.

VII. TEMPERATURE DEPENDENCE OF THE ATTACHMENT CROSS SECTION IN SF_6

The apparatus shown in Fig. 1 can also be used for a study of the temperature variation of attachment cross section in SF_6 in the temperature range 300-1300°K. Sulfur hexafluoride is an important material for quenching wakes and otherwise affecting the electron density in plasmas. The cause for this use is the extremely large cross section for negative ion formation near zero energy.

Figure 7 shows the SF_6^- current as a function of electron energy using the retarding-potential-difference method for limiting the energy spread of the electron beam. Also shown on Fig. 7 is an electron beam retarding curve taken simultaneously with the SF_6 signal. It can be seen that the peak of the SF_6^- signal occurs in the middle of the retarding curve, thus indicating that SF_6^- production occurs at zero energy. The cross section at this energy is about $10^{-14} cm^2$. Curves such as Fig. 7 are taken at various temperatures in the range 300-1300°K. No significant variation of the cross section is observed in this temperature range. This is shown in Fig. 8,

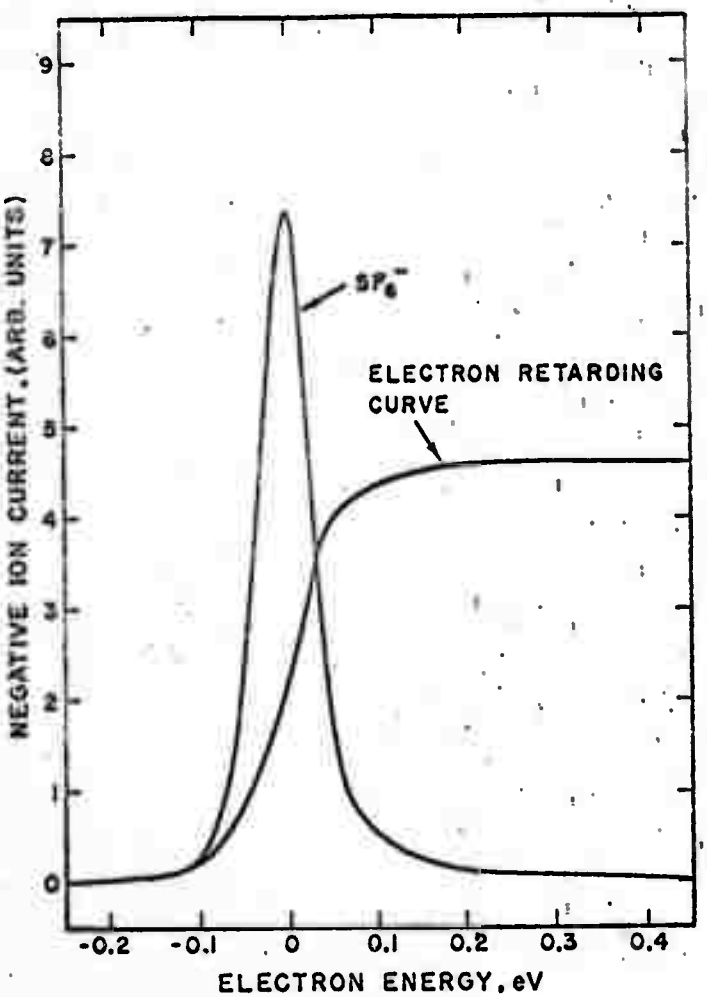

SF_6^- CURRENT AND ELECTRON RETARDING CURVE

Figure 7

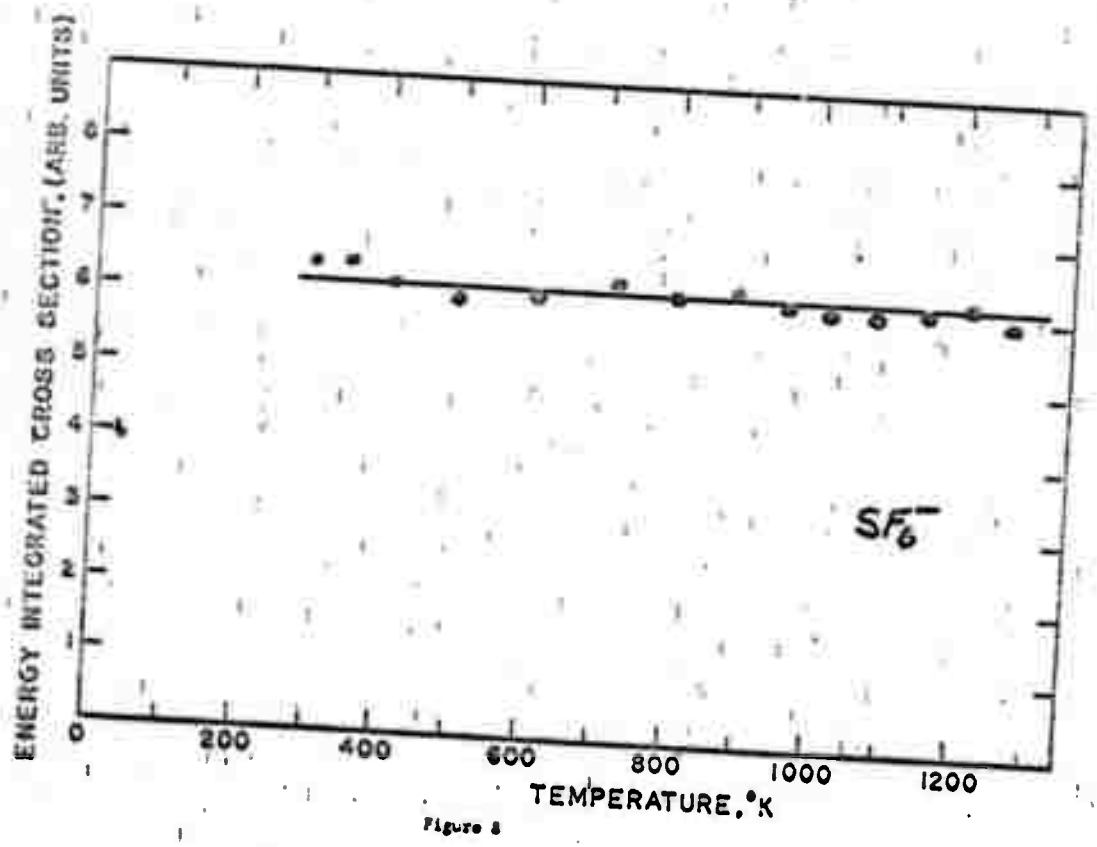

Figure 8

where the cross section is plotted as a function of gas temperature. Of course the energy distribution of the electrons remains independent of temperature.

Since the experiment measures the total negative ion signal, it is entirely possible that different product ions result at different temperatures. However, the total attachment cross section near zero energy remains constant. This result should be of interest in re-entry problems, where the gas temperature is far from room temperature.

VIII. EFFECT OF O_2 ON ATTACHMENT IN SF_6

We studied the effect of O_2 on the attachment cross section in SF_6. In practical applications, there are always atmospheric gases present when SF_6 is used for attachment. Therefore, it seemed advisable to see if O_2 would affect the attachment in SF_6. With SF_6 pressures in the 10^{-4} torr range and with O_2 pressures up to 20 times larger than the SF_6 pressures, no noticeable change in the effectiveness of SF_6 was found. This is shown in Fig. 9, where negative ion current (integrated over the electron energy distribution) is plotted vs. the ratio of O_2 density/SF_6 density. The curve is independent of the admixture of O_2 and we conclude that oxygen does not interfere with the efficient attachment of electrons to SF_6.

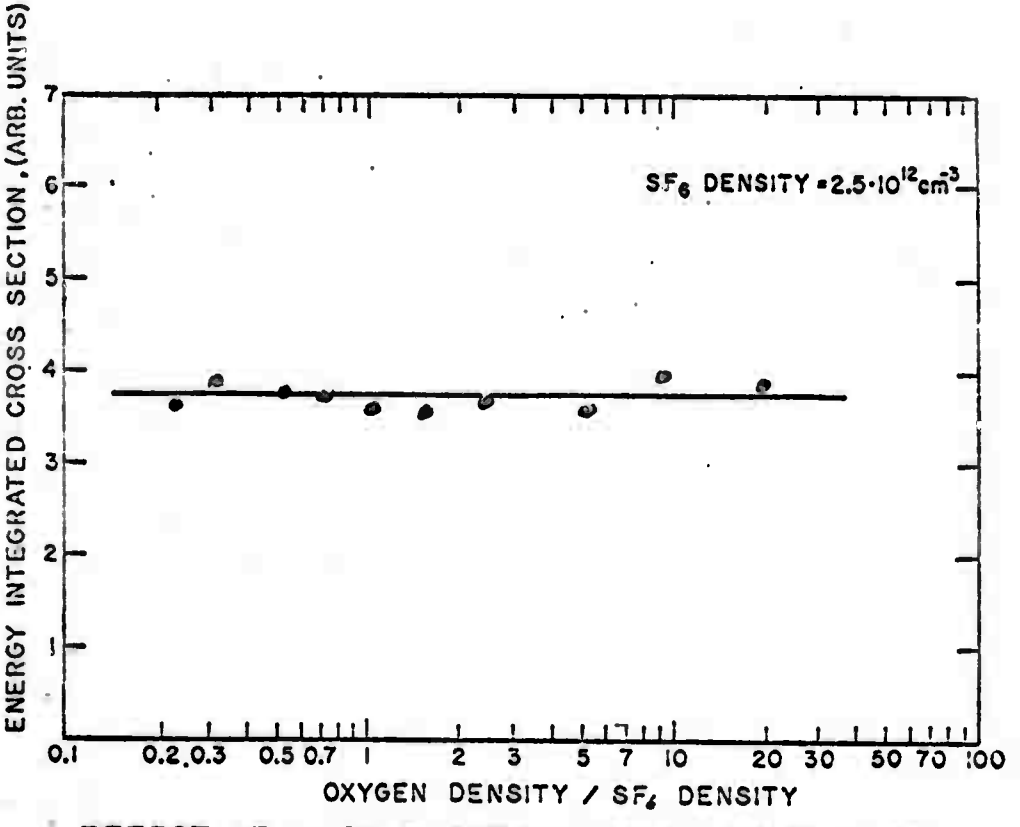

EFFECT OF O_2 ON ELECTRON ATTACHMENT IN SF_6 AT ZERO ELECTRON ENERGY

Figure 9

IX. TEMPERATURE DEPENDENCE OF THE ATTACHMENT CROSS SECTION IN CF_3Br

Besides SF_6, other quenching materials have been considered. One of the more interesting ones is CF_3Br, a trifluoromethyl halide. CF_3Br exhibits a cross section for negative ion formation near zero energy similar to SF_6. This is a desirable property for purposes of quenching. But the cross section near zero energy for CF_3Br is lower than that for SF_6 (see Sec. XIV). The energy dependence of the negative ion cross section as a function of electron energy is shown in Fig. 10. In sharp contrast to SF_6, we find a strong temperature dependence of the negative ion formation near zero electron energy. This is shown in Fig. 11. The cross section increases by a factor of almost 5 as the temperature is raised from 300°K to 950°K. The reason for the strong temperature dependence points to the possibility that negative ion formation near zero energy in CF_3Br is of a different nature than in SF_6.

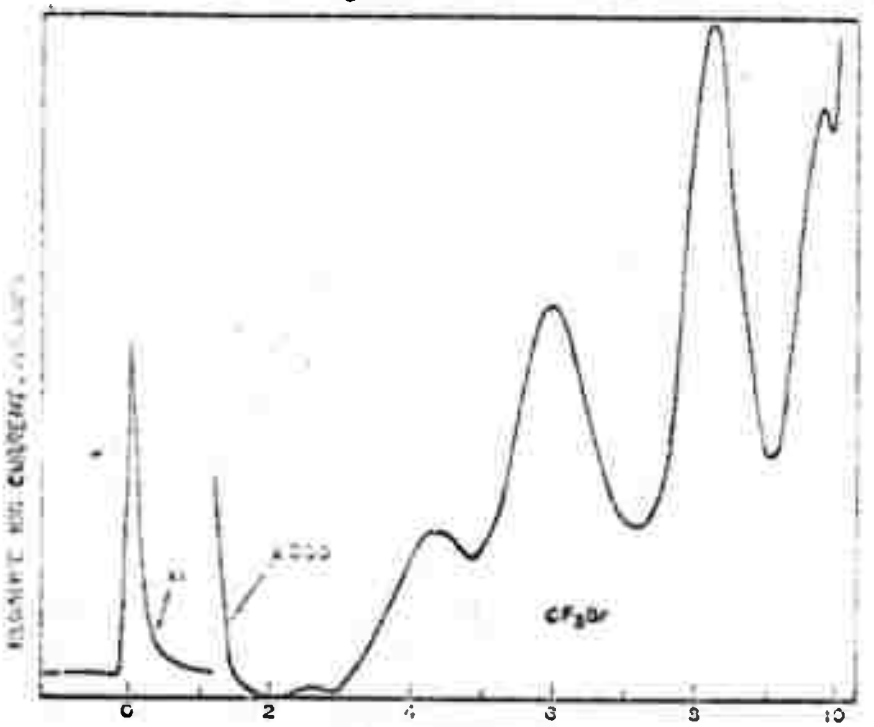

ENERGY DEPENDENCE OF NEGATIVE ION FORMATION IN CF_3Br

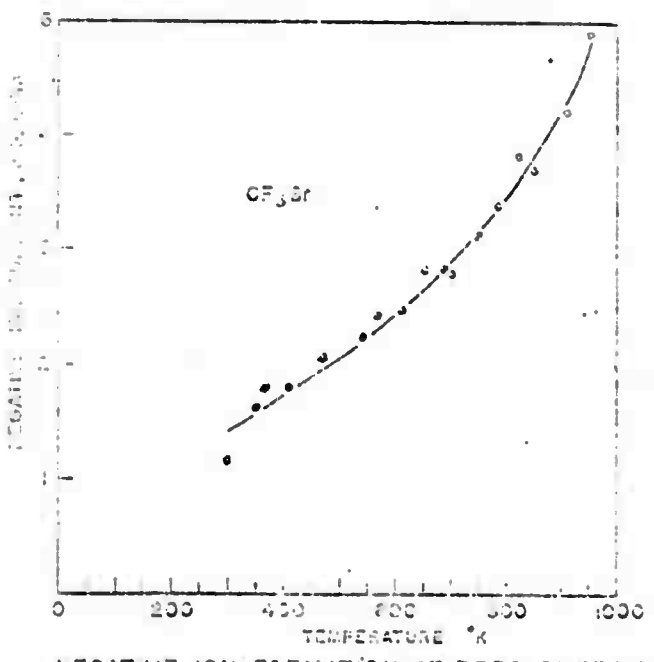

NEGATIVE ION FORMATION AT ZERO ENERGY
vs TEMPERATURE IN CF_3Br

Figure 11

In SF_6, the dominant attachment process at zero energy is the formation of a long-lived SF_6^- ion. In CF_3Br the dominant process near zero energy is probably dissociative attachment, i.e., the formation of F^- and Br^-. This has already been suggested by the work of J. Marriott and J. D. Craggs (J. Electron. Control 1, 405, 1956). Dissociative attachment processes near zero energy often exhibit strong temperature dependence, as evidenced by the O^- formation in N_2O, as studied by Chantry. One could argue that CF_3Br would be a preferable material for quenching since it leads to stable species of negative ions, whereas SF_6^- ejects the electron after about 25 μsec.

The work on CF_3Br is by no means complete. We have not done a mass spectrometer study to identify the peaks at 4, 6 and 8 eV shown in Fig. 10.

X. VIBRATIONAL CROSS SECTIONS IN O_2

For measurements of inelastic processes, the trapped-electron method is used. This method has a high sensitivity for the study of inelastic processes because all electrons which have made inelastic collisions are collected and measured. A detailed description of the trapped-electron method has been given previously [G. J. Schulz, Phys. Rev. 112, 150 (1958) and Phys. Rev. 116, 1141 (1959); also P. D. Burrow and G. J. Schulz. Phys. Rev. 187, 97 (1969)] and only the main points of the method will be given here.

The method consists of trapping low-energy electrons in an electrostatic well created on the axis of the tube shown in Fig. 1, and collecting them with high efficiency. Figure 12 shows the potential well created in the collision chamber. When a positive potential is applied to the collector M with respect to the collision chamber C, a potential well W is formed in the collision chamber, as shown in the lower portion of Fig. 12. The potential difference between electrodes P and C is denoted by V_a, and it can be seen that the electron energy in the collision chamber is V_a+W. The energy of the electrons as a function of position is indicated by the

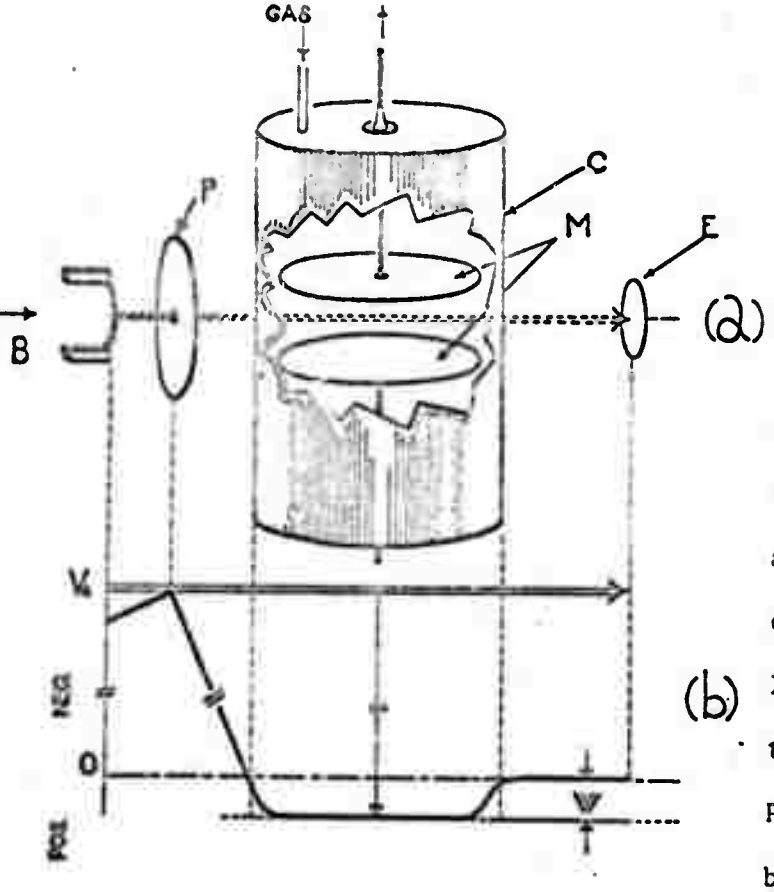

DIAGRAM OF APPARATUS (a) AND VARIATION OF POTENTIAL ALONG ELECTRON BEAM (b)

Figure 12

horizontal line. When electrons in the beam lose nearly all their energy in an inelastic collision, as they do when the incident electron energy is just above the threshold of excitation, they will end up in the potential well from which they cannot escape. These electrons will eventually migrate to the collector M where they are measured. Electrons which have lost energy less than V_a are not trapped and can reach the electron beam collector or the collision chamber walls.

Figure 13 shows a sampling of the primary data obtained in the present experiment. The figure shows the current received by the collector of trapped electrons as a function of the electron energy. Each curve is characteristic of a particular well depth, indicated on the figure. The well depth ranges from 5 mV to 160 mV. The first peak on each curve is the current resulting from elastic collisions. The reason for this peak is understood, but as far as the present experiment is concerned, its presence is not relevant. The remainder of the structure on each curve results from vibrational excitation of the molecules. The energy levels of the vibrational states of O_2 are indicated on the figure (v=1-4) as are the locations of the vibrational states of O_2^- (v'=5-11). The latter spacing (about 0.11 eV) has been determined in a separate experiment using the present apparatus.

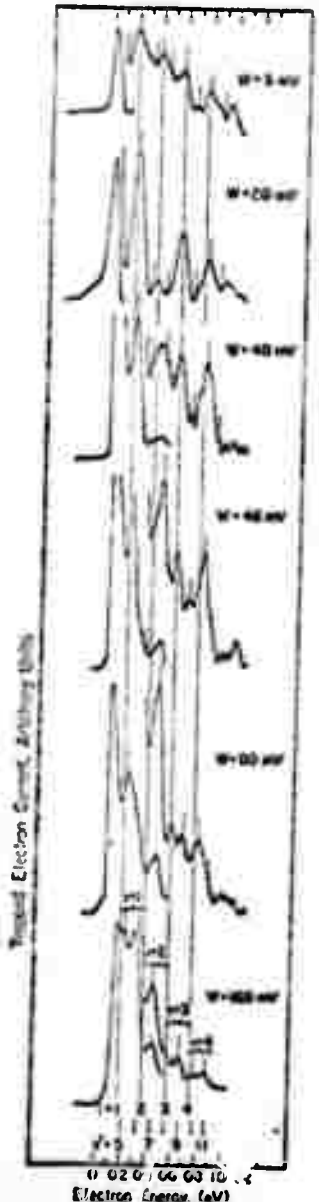

At low well depth, the spacing of the peaks corresponds to the spacing of the neutral molecule, whereas at the highest well depth, the spacing corresponds to the spacing of the O_2^-

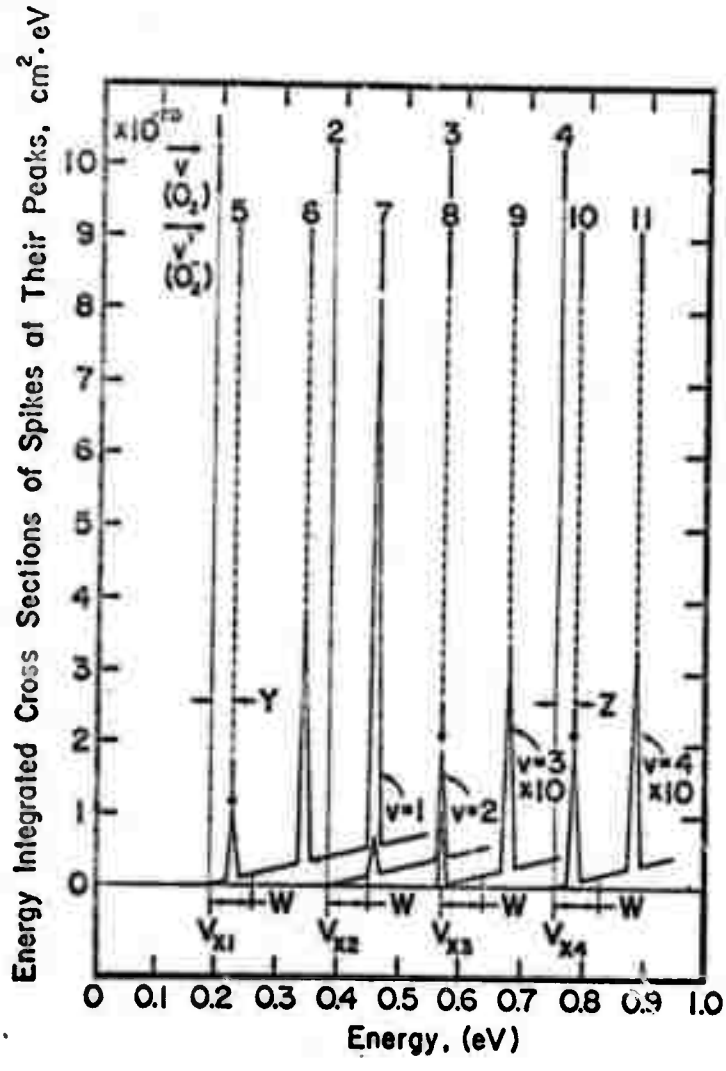

SHAPE OF CROSS SECTIONS FOR VIBRATIONAL EXCITATION IN O_2

Figure 14

from the fact that at low well depth, vibrational excitation proceeds via a "direct" process, wheras at the higher well depth vibrational excitation proceeds via a compound state, O_2^-. This effect can be best understood by considering Fig. 14, which shows the energy dependence of the vibrational cross section. This figure is derived from curves such as Fig. 13. The vibrational cross section consists of a slowly rising, "direct" component and a series of spikes at the location of the compound state. The width of the spikes drawn in Fig. 14 is somewhat arbitrary. Only the energy-integrated cross section of the spikes indicated on the ordinate of Fig. 14 is meaningful. The cross section scale is obtained in the present experiment by comparing the trapped-electron signal with the O^- signal resulting from dissociative attachment ($e + O_2 \rightarrow O^- + O$). The cross section for the latter process is $1.3 \times 10^{-18} cm^2$ at 6.7 eV. Figure 14 thus represents the best available cross section for vibrational excitation using electron beam experiments.

As a result of this work, we are also able to plot an energy level diagram of O_2 and O_2^- with the proper spacing and position of the vibrational states of O_2^-. This is shown in Fig. 15. The only parameter that does not result from the present experiment is the point at which we must cut off the sequence for O_2^-. This is the electron affinity of O_2, and Fig. 15 is drawn assuming that the value of the electron affinity of O_2 given by Pack and Phelps (0.43 eV) is correct.

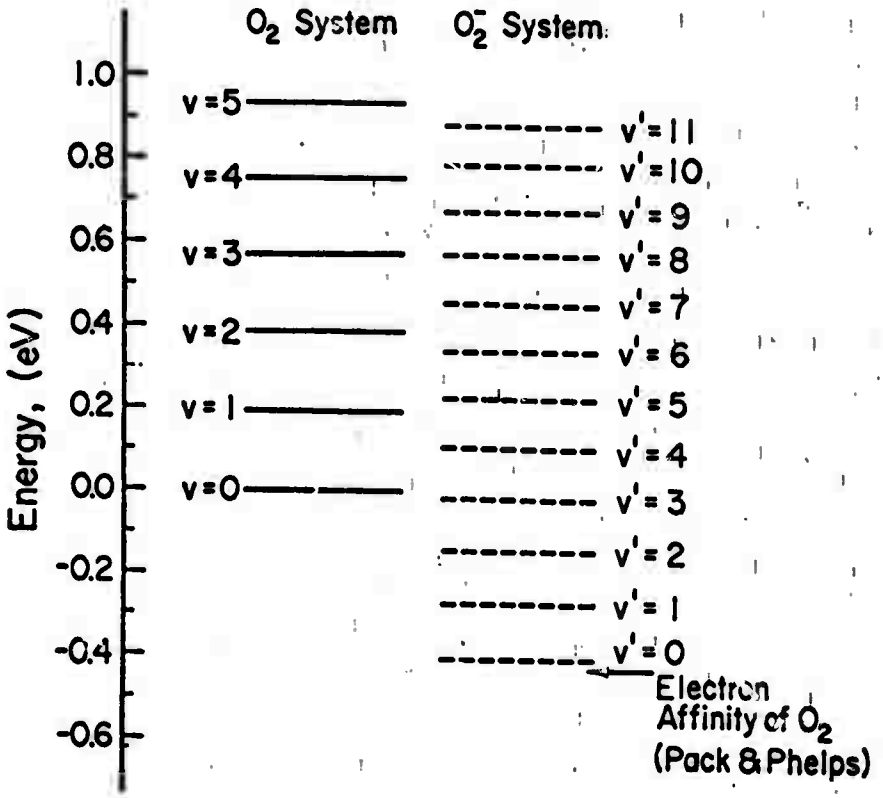

Vibrational Energy Levels of O_2 and O_2^-

Figure 15

XI. THREE-BODY ATTACHMENT IN O_2

Initial experiments on three-body attachment in O_2 using electron beam techniques have been performed. The negative ion current of O_2^-, resulting from three-body attachment, has been measured in the energy range 0-1 eV. The pressure dependence is found to be quadratic, as expected for a three-body reaction. The ratio of the peak O_2^- current, which occurs at 0.1 eV, to O^- current at 6.7 eV (i.e., the peak of the dissociative attachment cross section) has a linear dependence on pressure and can be used for absolute calibration, together with a knowledge of the absolute density in the oven.

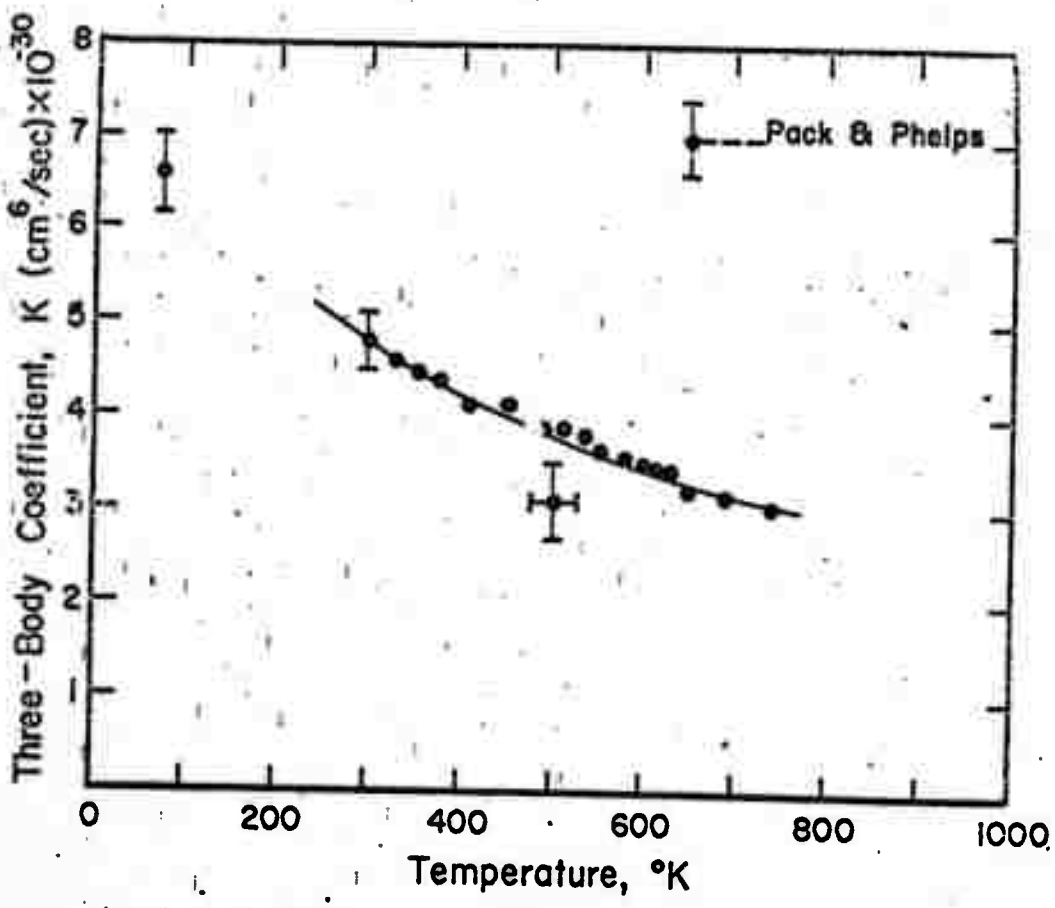

TEMPERATURE DEPENDENCE OF THREE-BODY ATTACHMENT IN O

We find that the peak three-body attachment cross section at 0.1 eV decreases as the gas temperature is increased. Between 300°K and 750°K the curve follows a $T^{-\frac{1}{2}}$ form, the value at 750°K being 62% of the value at 300°K. (See Fig. 16.)

The theory for three-body attachment was developed by Herzenberg. It accepts the Bloch-Bradbury model of a two-stage process, namely

[1] $e + O_2 \rightarrow O_2^{-*} + O_2$ (resonance attachment)

[2] $O_2^{-*} + O_2 \rightarrow O_2^{-} + O_2$ (stabilization)

Modern resonance theory, developed in the last few years, is applied to the capture process [1]. Thus, the capture process is described using the Breit-Wigner resonance theory which gives the energy dependence of the initial capture cross section in terms of the width of the compound state.

The stabilization process [2] has the following competing reaction scheme:

[2] $O_2^{-*} + O_2 \rightarrow O_2^{-} + O_2$ (stabilization)

[3] $\rightarrow O_2^{-*} + O_2$ (elastic)

[4] $\rightarrow O_2 + O_2 + e$ (detachment)

[5] $\rightarrow O_4 + e$ (associative detachment)

In the theory outlined above, the temperature dependence of the three-body attachment process comes from the process competing with stabilization (reactions [2] - [5]).

XII. VIBRATIONAL CROSS SECTIONS IN NO

The method of study described in Section X, namely the trapped-electron method, was applied to a study of the vibrational cross section in NO. The molecule NO has a much lower electron affinity (about 0.05 eV) than O_2 and it possesses a dipole moment. The trapped-electron spectrum is shown in Fig. 17. Noteworthy is the spectrum at low well depth (W<10 mV) which shows only peaks due to the excitation of the 1st and 4th vibrational states in NO. Peaks resulting from the excitation of the 2nd and 3rd vibrational states are absent, although they do appear at the higher well depths. (The small numbers in the circles, under each peak, indicate the vibrational state involved, and the scale marked v'=0-10 indicates the location of the compound states.) These observations are indicative of a coincidence in energy levels between the 4th vibrational state of NO and one of the states (v'=6) of NO^-. This coincidence of energy levels allows us to draw a reliable energy level diagram of NO^-, shown in Fig. 18. Here, we show the coincidence of the levels v=4 and v'=6 and we use the spacing of vibrational levels of NO^-, determined in a separate experiment

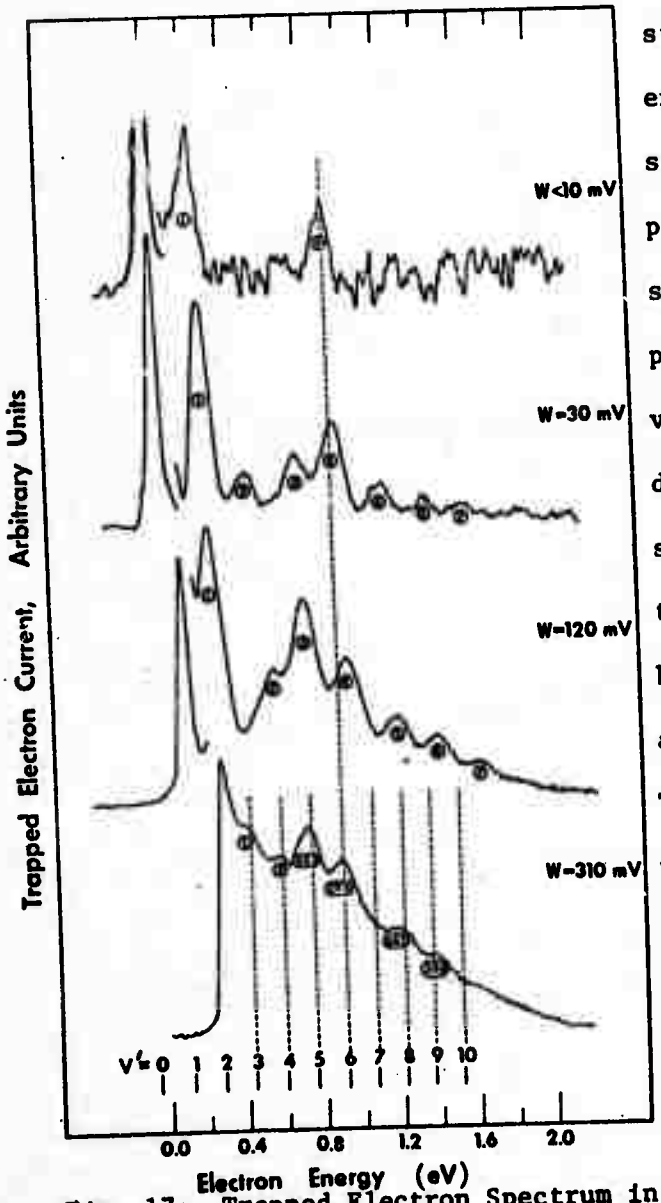

Fig. 17: Trapped Electron Spectrum in NO

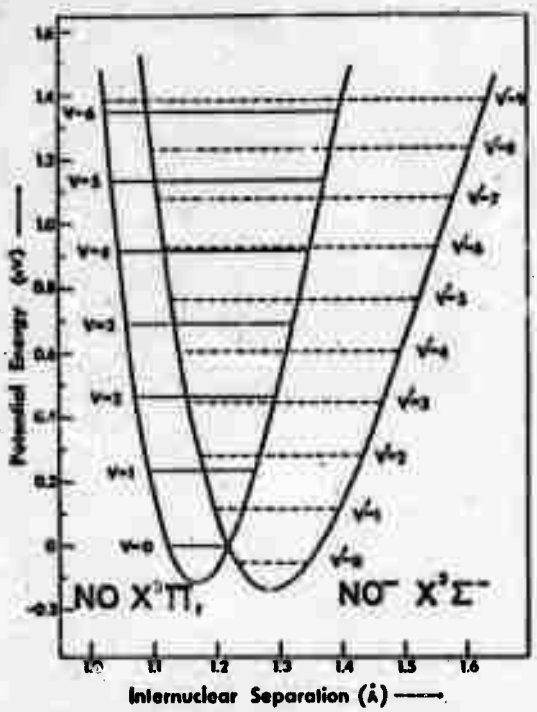

Fig. 18: Potential Energy Diagram of NO, Deduced From Present Experiment

on the elastic scattering of electrons on NO at low energy. This elastic cross section exhibits structure characteristic of the vibrational states in NO^-.

Our final estimate of the vibrational cross section as a function of energy is shown in Fig. 19. The absolute magnitude of the cross section is determined from a known positive-ion cross section, and the width of the peaks corresponds to the width of the peaks observed in elastic scattering. The lifetime of the vibrational states of NO^- is shorter than the corresponding lifetimes of O_2^-, and thus the width of the levels is larger.

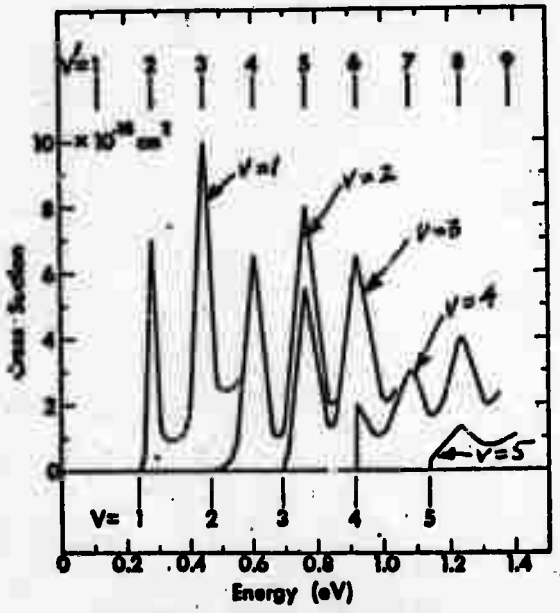

Fig. 19: Vibrational Cross Section in NO

XIII. DETECTION OF VIBRATIONALLY EXCITED N_2 BY SUPERELASTIC ELECTRON IMPACT

This work was undertaken in order to develop a tool for the measurement of the density of excited species, in order to study the transfer of electronic excitation of atoms into vibrational excitation of molecules, and in order to study some cross sections which are difficult to study by other means. In a superelastic collision, an electron colliding with an excited atom or molecule gains kinetic energy and leaves the atom or molecule in a lower energy state. Superelastic electrons are observed from collisions with vibrationally excited N_2 molecules in their ground electronic state. Vibrationally excited N_2 is produced by the quenching of optically excited Rb vapor. Rubidium resonance radiation is incident on a collision chamber containing Rb vapor and N_2. A fraction of the excited $Rb(^2P_{1/2,3/2})$ atoms produced by photon absorption collide with N_2 and are quenched with high efficiency. As a result of the quenching, vibrationally excited N_2 is produced. A low-energy electron beam is passed through the collision chamber, and those electrons making superelastic collisions are analyzed. Preliminary information is obtained on the transfer of Rb electronic energy into vibrational energy of N_2.

The apparatus is shown in Fig. 20. Plates S_1 through S_5 form an electron gun which may be operated in the retarding-potential-difference mode. Typical electron beam currents of 5×10^{-8} A with a resolution of 0.2 eV at half-maximum are used. The electron beam is collimated by a uniform axial magnetic field of 180 G. A retarding voltage may be applied to electrode

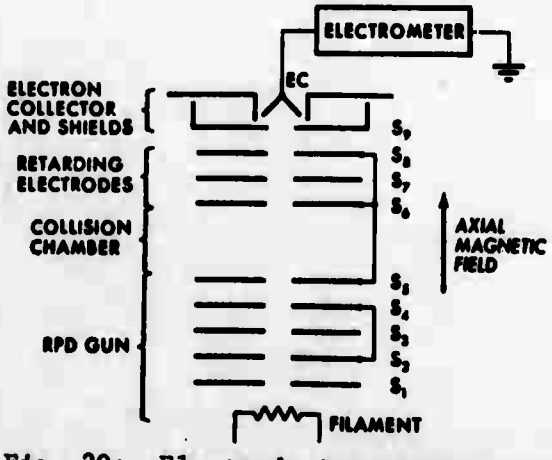

Fig. 20: Electrode Arrangement for

S_7, to analyze the energy of the electrons. The electron current transmitted past the retarding plate is collected at EC and measured with a vibrating-reed electrometer.

The collision chamber is surrounded by a concentric quartz cylinder which admits Rb resonance radiation at 7800 and 7948 Å from three low-pressure Osram arc lamps positiond around the cylinder. The lamps are modified to include a cooling system which decreases the self-reversal of the resonance lines. Approximately 10^{18} photons per second of resonance light are delivered into the collision chamber. The tube and the side arm containing Rb are kept at a temperature such that the vapor pressure in the collision chamber is about 10^{-4} Torr. At this pressure all of the resonance light is absorbed. The nitrogen pressure is in the region of 10^{-2} Torr and is monitored by the fractional attenuation of the main electron beam.

Since the energy levels of $Rb(^2P_{1/2,3/2})$ lie at 1.57 and 1.59 eV, respectively, quenching into vibrational levels of N_2 up to v=5 is energetically allowed. However, it is only possible for us at present to observe superelastic transitions for the v=5 level to the ground state of N_2. The results are shown in Fig. 21. We conclude from an analysis of these experiments that the superelastic method for detection of excited species works fairly well and that the quenching cross section of excited Rb into the v=5 level of N_2 yields a value approximately equal to the total quenching cross section (about 4×10^{-15} cm^2).

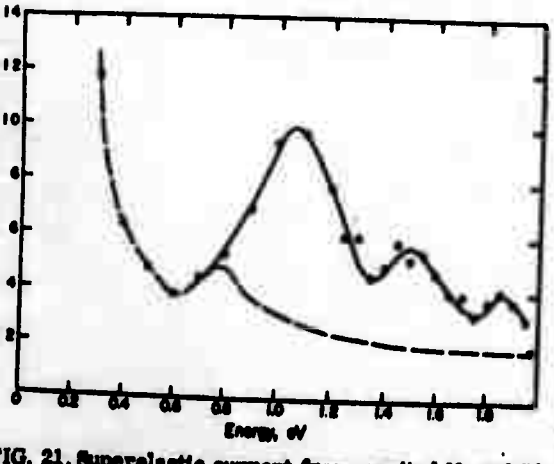

FIG. 21. Superelastic current from excited N_2 and Rb as function of incident electron energy. The broken shows the contribution from excited Rb.

XIV. ABSOLUTE CROSS SECTIONS FOR NEGATIVE ION FORMATION NEAR ZERO ENERGY IN SF_6, $CC\ell_4$, $CFC\ell_3$, CH_2Br_2, CH_3I, $CHC\ell_3$, CF_3Br, CH_3Br

The absolute energy-integrated cross sections for negative ion formation for the above-named molecules are shown in Fig. 22. The strong temperature dependence of these cross sections is obvious from the figure. It appears that all the molecules approach a common value for the negative ion cross section as the temperature is raised. This common value is in the neighborhood of the theoretical maximum of this cross section. It should be noted that the negative ions formed near zero energy have not been analyzed in the present experiment, although such an analysis is contemplated. The stability, i.e. the electron affinity, of the product ions may be important for understanding the quenching properties of the different molecules.

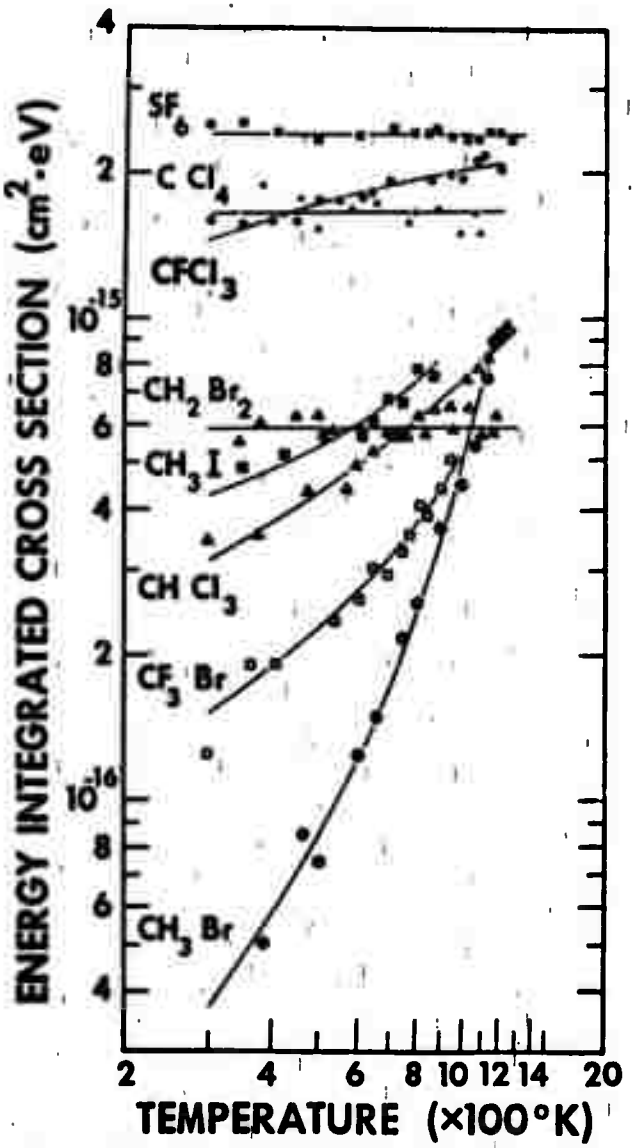

Fig. 22: Energy-integrated cross section for negative-ion formation near zero energy, vs gas temperature. The molecules selected are of interest for quenching of wakes.

XV. ABSOLUTE INELASTIC CROSS SECTIONS FOR N_2 and CO_2 IN THE 2-4 EV RANGE

Using the trapped-electron method, we have measured the magnitude of the total inelastic sections in the region of the low-lying compound states in N_2 and CO_2. This is the energy regime in which the vibrational cross section is very large as a result of the decay of the compound state. The dominant inelastic process is vibrational excitation. We find a cross section of 6.0×10^{-16} cm^2 for N_2 at 2.3 eV and a cross section of 8.3×10^{-16} cm^2 at 3.8 eV in CO_2. The latter value is almost an order of magnitude larger than previously published values. The value in N_2 is in excellent agreement with the analysis of swarm experiments (A. G. Engelhardt, A. V. Phelps and C. G. Risk, Phys. Rev. 135, A 1556, 1964). The values quoted above are needed for an analysis of laser-type discharges in N_2 - CO_2 mixtures. Also, vibrational excitation is believed to be a dominant electron energy loss mechanism in Martian and Venusian atmospheres.

XVI. PUBLICATIONS UNDER PRESENT CONTRACT

P. D. Burrow and Paul Davidovits, "Detection of Vibrationally Excited N_2 by Superelastic Electron Impact," Phys. Rev. Letters 21, 1789 (1968).

M. J. W. Boness and G. J. Schulz, "Vibrational Excitation of CO_2 by Electron Impact," Phys. Rev. Letters 21, 1031 (1968).

A. Herzenberg, "The Attachment of Slow Electrons to O_2 Molecules," J. Chem. Phys. 51, 4942 (1969).

P. D. Burrow and G. J. Schulz, "Vibrational Excitation by Electron Impact Near Threshold in H_2, D_3, N_2 and CO." Phys. Rev. 187, 97 (1969).

D. Spence and G. J. Schulz, "Vibrational Excitation by Electron Impact in O_2," Phys. Rev. A 2, 1802 (1970).

D. Spence and G. J. Schulz, "Vibrational Excitation and Compound States in NO," Phys. Rev. A 3, 1968 (1971).

D. Spence and G. J. Schulz, "Three-body Attachment in O_2 Using Electron Beams," Phys. Rev. A 5, 2 (1972).

D. Spence, J. L. Mauer and G. J. Schulz, "Measurement of Total Inelastic Cross Section for Electron Impact in N_2 and CO_2," (submitted to J. Chem. Phys.).